Communications in Nonlinear Science and Numerical Simulation 125 (2023) 107380

Contents lists available at ScienceDirect

Communications in Nonlinear Science and Numerical Simulation

journal homepage: www.elsevier.com/locate/cnsns

Research paper

Synchronization and multistability in a network of diffusively coupled laser models

Mahtab Mehrabbeik [a], Sajad Jafari [a,b], Riccardo Meucci [c], Matjaž Perc [d,e,f,g,h,*]

[a] Department of Biomedical Engineering, Amirkabir University of Technology (Tehran Polytechnic), Tehran, Iran
[b] Health Technology Research Institute, Amirkabir University of Technology (Tehran Polytechnic), Tehran, Iran
[c] Istituto Nazionale di Ottica—CNR, Largo E. Fermi 6, 50125 Firenze, Italy
[d] Faculty of Natural Sciences and Mathematics, University of Maribor, Koroška cesta 160, 2000 Maribor, Slovenia
[e] Department of Medical Research, China Medical University Hospital, China Medical University, Taichung 404332, Taiwan
[f] Alma Mater Europaea, Slovenska ulica 17, 2000 Maribor, Slovenia
[g] Complexity Science Hub Vienna, Josefstädterstraße 39, 1080 Vienna, Austria
[h] Department of Physics, Kyung Hee University, 26 Kyungheedae-ro, Dongdaemun-gu, Seoul, Republic of Korea

ARTICLE INFO

Article history:
Received 1 November 2022
Received in revised form 8 April 2023
Accepted 15 June 2023
Available online 19 June 2023

Keywords:
Synchronization
Chimera
Multistability
Laser network

ABSTRACT

Synchronization phenomena refer to the emergence of common temporal patterns among clusters of interacting units in a complex network. In information transmission, lasers' synchronization plays a key role in facilitating information communication. This paper is devoted to studying the synchronization of globally coupled identical laser models via the linear and nonlinear forms of diffusive couplings. In this regard, the master stability function and time-averaged synchronization error are employed as the analytical and numerical approaches to examine complete synchronization. Apart from the complete synchrony, the constructed networks are explored to find other synchronization patterns and multistability. The results obtained from the master stability function analysis, which are further approved by the numerical outcomes, show that when coupled through the linear diffusive function, the interacting laser models achieve complete synchrony in a small value of the coupling parameter. However, in the nonlinear case, complete synchronization cannot be attained. Moreover, multistability can be observed in different network states, including cluster synchronization, chimera, and solitary states.

1. Introduction

In real-world applications, many systems can be found consisting of highly interconnected units, such as biological systems and the Internet network [1] or coupled mechanical systems [2]. Such interactive units can exhibit various collective dynamics. Nonetheless, collective behaviors gain significance when all or some units share a typical temporal pattern called synchronization [3]. Synchronization is a consequence of adding a forcing term to the systems or coupling them in a particular structure [4]. Thus, the emergence of the synchronization phenomena might lead to a specific process or have a notable significance. For instance, from an information processing perspective, the synchronization of chaotic circuits brings high-rate and secure communications opportunities [5,6].

* Corresponding author at: Faculty of Natural Sciences and Mathematics, University of Maribor, Koroška cesta 160, 2000 Maribor, Slovenia.
E-mail address: matjaz.perc@gmail.com (M. Perc).

https://doi.org/10.1016/j.cnsns.2023.107380
1007-5704/

Different types of synchronization have been defined based on experimental and practical observations as well as simulated outcomes [7,8]. Complete synchronization, referring to the state wherein all interacting units form a coherent cluster, is the most known type of synchronization [9]. In complex network analysis, complete synchronization can be analyzed numerically and analytically through the master stability functions (MSFs) developed by Pecora and Carroll [10] in 1998. Due to the importance of complete synchronization emergence in complex networks, many studies have been conducted to examine the synchronization of dynamical systems in different fields [11–13]. Nevertheless, before reaching complete synchrony, different collective dynamics, including chimera [14,15], solitary state [16], cluster synchronization [17], phase synchronization [18], and lag synchronization [19], are feasible.

Chaotic dynamics in lasers have been primarily investigated in the last decades, including experimental investigations and numerical investigations on suitable models. For instance, Haken developed a mathematical single-mode laser model. Agrawal [20] came up with a mathematical model of semiconductor lasers. Ciofini et al. [21] introduced the four-level CO_2 laser model. Meucci et al. [22] proposed a CO_2 laser model with minimal nonlinearity and feedback. After the seminal paper on chaos synchronization [23], lasers continue to play a crucial role in showing how their synchronization can be used in communicating information in both digital and analog forms [24]. Different studies have been elaborated on the synchronization of laser models. For example, Sugawara et al. [25] experimentally and mathematically observed synchronization in a network of two lasers coupled in the master–slave configuration. More clearly, they studied the synchronization of two coupled CO_2 laser models, one of which (slave) was driven by the output of the other (master). The authors found the entrainment of chaos when there was a slight difference between the master and slave systems' solutions. Employing the nonautonomous, periodically forced CO_2 laser model, Mariño et al. [26] also gave evidence of synchronization in a structure consisting of a master and a slave laser model. By calculating the synchronization error, they found the criteria (the proper value of the coupling strength) for synchronizing two coupled periodically-forced CO_2 laser models. DeShazer et al. [27] observed phase synchronization in an array of three chaotic lasers. According to their results, to asses phase synchronization, the numerical measure plays an important role. The observation of in-phase and anti-phase synchronization between two Semiconductor quantum dot lasers coupled through the beating of lasing modes was reported by Hillbrand et al. [28]. They experimentally showed that both states could occur in the same configuration by changing the damping losses. In the study conducted by Mihana et al. [29], the lag synchronization of three lasers configurated in an undirected ring network was used as the basis of a decision-making operation. The three laser models were unidirectionally coupled in their studied network with a predetermined time delay and different coupling strengths. The emergence of cluster synchronization and chimera in a network of delay-coupled lasers was also reported by Zhang et al. [30]. They mainly focused on the formation of synchronous and asynchronous clusters in random and power grid networks. The formation of such synchronous clusters in a complex network of coupled lasers was also announced by Kouomou and Woafo [31]. In this study, the authors considered a lattice (two-dimensional network configuration) network of chaotic current-modulated semiconductor lasers coupled through linear diffusive functions and studied the synchronization patterns in the constructed network. Röhm et al. [32] also found the chimera state in a fully connected network of delay-coupled lasers. This study examined the formation of the synchronization patterns in a network of four laser models.

The laser model investigated in the current study has had a tremendous impact since it highlighted both deterministic chaos and multistability for the first time, recently proposed in [33]. Considering the enormous impact of multistability in various fields, even very distant from laser physics, we believe that the synchronization in this model has a very general character. In network analysis, the diffusive coupling functions in fully connected units are the most common example of shift-invariant couplings [34]. Thus, this paper investigates the synchronization analytically using the MSF analysis and numerically using the time-averaged synchronization error in a network of globally coupled laser models with linear and nonlinear diffusive coupling functions. The built network is also explored in-depth to find other synchronization patterns and multistability. In Section 2, the mathematical definition of the studied network is given in detail. Section 3 includes the analytical and numerical results obtained as a consequence of applying linear and nonlinear diffusive coupling functions. In the end, the conclusions are presented in Section 4.

2. The network model

Considering pairwise connections, the network of globally coupled oscillators can be expressed as

$$\dot{\boldsymbol{X}}_i = \boldsymbol{F}(\boldsymbol{X}_i) + \epsilon \sum_{j=1}^{N} G_{ij} \boldsymbol{H}(\boldsymbol{X}_i, \boldsymbol{X}_j), \tag{1}$$

where $i = 1, 2, \ldots, N$, N is the network size, $\boldsymbol{X}_i = [x_i, y_i]$ is the state vector, $\boldsymbol{F}(\boldsymbol{X}_i)$ describes the dynamics of the system considered as the ith node of the network, ϵ is the coupling parameter, G is the connectivity matrix describing the global/all-to-all network structure, and $\boldsymbol{H}(\boldsymbol{X}_i, \boldsymbol{X}_j)$ defines the coupling function. Note that $G_{ij} = 1$ indicates that the ith and jth oscillators are connected through a link. For any node, $\boldsymbol{F}(\boldsymbol{X}_i)$ follows the dynamics of the two-level laser model, proposed by Meucci et al. [33], which is mathematically described as

$$\boldsymbol{F}(\boldsymbol{X}_i) = \begin{cases} f(x_i, y_i) = -x_i(1 + kI_m^2 - y_i) \\ g(x_i, y_i) = -\gamma y_i - \alpha x y_i + \gamma p_0 \end{cases}, \tag{2}$$

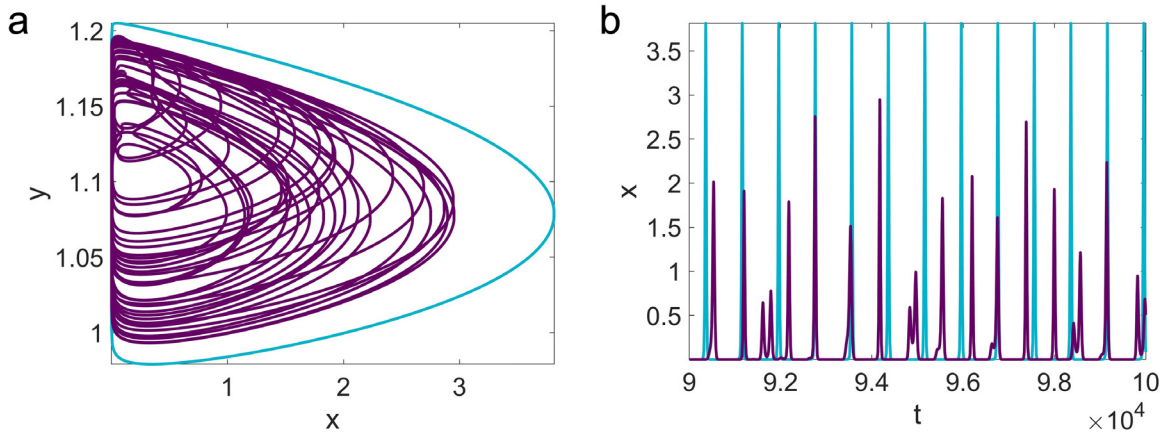

Fig. 1. (a) The phase portraits and (b) the temporal pattern of a single node dynamics described by the two-level laser model. The parameters are set at $k = 12$, $\Gamma = 0.0025$, $B_0 = 0.1$, $m = 0.02$, $f_{mod} = 0.005$, and $\alpha = 0.002$. The initial conditions are $(x_0, y_0) = (1, 1)$ for the chaotic attractor (shown in royal purple), and $(x'_0, y'_0) = (2, 1)$ for the limit cycle (shown in aqua blue). Each node exhibits a chaotic solution in coexistence with a period-1 limit cycle in this set of parameters.

where x is a fast variable indicating the laser intensity, the term $k_0(1 + kI_m^2)$ is the decay rate of the fast variable x with non-modulated cavity loss k_0 and modulation depth k. Here, $k_0 = 1$ is consiered. Also, $I_m = B_0 + m\sin(2\pi f_{mod}t)$ is the time-dependent modulation sinusoidal signal with the bias of B_0, the amplitude of m, and the frequency of f_{mod}. On the other hand, y denotes the slow variable reflecting the population inversion with a decay rate γ. Moreover, p_0 is the normalized pump strength and α is the normalization factor of the fast variable x. Supposing the identical dynamics for the network's nodes, the model's parameters are set at $k = 12$, $\gamma = 0.0025$, $B_0 = 0.1$, $m = 0.02$, $f_{mod} = 0.005$, and $\alpha = 0.002$, wherein the original system is bistable (the coexistence of a strange attractor and a period-1 limit cycle). Fig. 1 demonstrates the phase portraits and the temporal pattern of a single node dynamics (the two-level laser model) set at the aforementioned parameters with the initial condition of $(x_0, y_0) = (1, 1)$ for the chaotic attractor (shown in royal purple), and $(x'_0, y'_0) = (2, 1)$ for the limit cycle (shown in aqua blue).

In this paper, a network of globally coupled oscillators ($N = 100$) is considered under two types of coupling functions $\boldsymbol{H}(\boldsymbol{X}_i, \boldsymbol{X}_j)$, including linear diffusive and nonlinear diffusive coupling functions.

3. Results

The constructed network, described in Network (1), is explored in terms of synchronization, chimera, and multistability under two different coupling functions (linear and nonlinear). For each scenario, the synchronization is investigated analytically, using the MSF formalism [35], and numerically using the time-averaged synchronization error described as

$$E = \left\langle \frac{1}{N-1} \sum_{\substack{j=1 \\ i \neq j}}^{N} \left\| \boldsymbol{X}_j(t) - \boldsymbol{X}_i(t) \right\| \right\rangle_t , \tag{3}$$

where N is the network size, $\langle . \rangle$ is the symbol of time averaging, and $\|.\|$ is the symbol of Euclidean norm.

3.1. Linear diffusive coupling function

In the first scenario, the oscillators are considered to be globally coupled through the linear diffusive function. Thus, Network (1) can be rewritten as

$$\dot{\boldsymbol{X}}_i = \begin{cases} \dot{x}_i = -x_i(1 + kI_m^2 - y_i) \\ +\epsilon \sum_{j=1}^{N} G_{ij}(x_j - x_i) \\ \dot{y}_i = -\gamma y_i - \alpha x y_i + \gamma p_0 \end{cases} . \tag{4}$$

Hence, in this case, the coupling function $\boldsymbol{H}(\boldsymbol{X}_i, \boldsymbol{X}_j)$ reads

$$\boldsymbol{H}(\boldsymbol{X}_i, \boldsymbol{X}_j) = [x_j - x_i, 0]. \tag{5}$$

In order to analyze the synchronization of the studied network analytically, the MSF analysis is performed on Network (4). In the synchronization manifold $\boldsymbol{X}_s$ ($\boldsymbol{X}_s = (x_s, y_s)$), the state variables of all oscillators attain the same temporal

solution. Therefore, deeming $\boldsymbol{X}_1 = \boldsymbol{X}_2 = \cdots = \boldsymbol{X}_{N-1} = \boldsymbol{X}_N = \boldsymbol{X}_s$, and thus $\boldsymbol{H}(\boldsymbol{X}_i, \boldsymbol{X}_j) \equiv 0$, the synchronization manifold becomes

$$\boldsymbol{F}(\boldsymbol{X}_s) = \begin{cases} f(x_s, y_s) = -x_s(1 + kl_m^2 - y_s) \\ g(x_s, y_s) = -\gamma y_s - \alpha x y_s + \gamma p_0 \end{cases}, \tag{6}$$

which is similar to a single oscillator dynamics. To perform the MSF analysis, a small perturbation $\delta\boldsymbol{X}_i$ is added to the synchronization manifold for each oscillator. Accordingly, we have $\delta\boldsymbol{X}_i = \boldsymbol{X}_i - \boldsymbol{X}_s$, where $\delta\boldsymbol{X}_i = (\delta x_i, \delta y_i)$. Therefore, the dynamics of the variational equations can be obtained through

$$\begin{aligned} &\delta\dot{\boldsymbol{X}}_i = \boldsymbol{DF}(\boldsymbol{X}_s)\delta\boldsymbol{X}_i + \\ &\epsilon \sum_{j=1}^{N} G_{ij} \left[\left. \frac{\partial \boldsymbol{H}}{\partial \boldsymbol{X}_i} \right|_{(\boldsymbol{X}_s, \boldsymbol{X}_s)} \delta\boldsymbol{X}_i + \left. \frac{\partial \boldsymbol{H}}{\partial \boldsymbol{X}_j} \right|_{(\boldsymbol{X}_s, \boldsymbol{X}_s)} \delta\boldsymbol{X}_j \right], \end{aligned} \tag{7}$$

where $\boldsymbol{DF}(\boldsymbol{X}_s)$ is the Jacobian matrix of $\boldsymbol{F}(\boldsymbol{X}_s)$. Supposing $\boldsymbol{H}(\boldsymbol{X}_i, \boldsymbol{X}_j)$ as Eq. (5), the variational equation described in Eq. (7) changes into

$$\delta\dot{\boldsymbol{X}}_i = \begin{cases} \delta\dot{x}_i = Df(\boldsymbol{X}_s)\delta\boldsymbol{X}_i \\ +\epsilon \sum_{j=1}^{N} G_{ij} \left(\delta x_j - \delta x_i\right) \\ \delta\dot{y}_i = Dg(\boldsymbol{X}_s)\delta\boldsymbol{X}_i \end{cases}. \tag{8}$$

Assuming A as the diagonal matrix whose elements on the main diagonal are the degrees corresponding to each node, the Laplacian matrix L satisfies $L = A - G$. Consequently, $\delta\dot{x}_i$ described in Eq. (8) can be written in terms of the Laplacian matrix L as follows

$$\begin{aligned} &\delta\dot{x}_i = Df(\boldsymbol{X}_s)\delta\boldsymbol{X}_i + \epsilon \sum_{j=1}^{N} G_{ij}\delta x_j - \epsilon \sum_{j=1}^{N} G_{ij}\delta x_i \\ &= Df(\boldsymbol{X}_s)\delta\boldsymbol{X}_i + \epsilon \left(\sum_{j=1}^{N} A_{ij}\delta x_j - \sum_{j=1}^{N} L_{ij}\delta x_j \right) \\ &-\epsilon\delta x_i \sum_{j=1}^{N} G_{ij} \\ &= Df(\boldsymbol{X}_s)\delta\boldsymbol{X}_i + \epsilon \left((N-1)\delta x_i - \sum_{j=1}^{N} L_{ij}\delta x_j \right) \\ &-\epsilon(N-1)\delta x_i \\ &= Df(\boldsymbol{X}_s)\delta\boldsymbol{X}_i - \epsilon \sum_{j=1}^{N} L_{ij}\delta x_j. \end{aligned} \tag{9}$$

The block diagonally coupled Eq. (9) can be expressed in block diagonally decoupled form by diagonalizing the eigenvalues of the Laplacian matrix L. Hence,

$$\delta\dot{\boldsymbol{X}}_i = \begin{cases} \delta\dot{x}_i = Df(\boldsymbol{X}_s)\delta\boldsymbol{X}_i - \epsilon\lambda_i\delta x_i \\ \delta\dot{y}_i = Dg(\boldsymbol{X}_s)\delta\boldsymbol{X}_i \end{cases}, \tag{10}$$

where λ_i is the eigenvalues of the Laplacian matrix L. Assuming $\delta\boldsymbol{X}_i : (\delta x_i, \delta y_i) \rightarrow \boldsymbol{\zeta}_i : (\zeta_i^x, \zeta_i^y)$ and $K_i = \epsilon\lambda_i$ as the normalized coupling parameter, the variational equation becomes

$$\delta\dot{\boldsymbol{\zeta}}_i = \begin{cases} \delta\dot{\zeta}_i^x = f_x\zeta_i^x + f_y\zeta_i^y - K_i\zeta_i^x \\ \delta\dot{\zeta}_i^y = g_x\zeta_i^x + g_y\zeta_i^y \end{cases}. \tag{11}$$

Since the considered network is homogeneous with global connections, we have $\lambda_1 = 0$, and $\lambda_2 = \lambda_3 = \cdots = \lambda_{N-1} = \lambda_N = N$. The maximum Lyapunov exponent (MLE) of Network (11) leads to the MSF (Ψ). Generally, when $\Psi < 0$ for all λ_i, where $i = 2, \ldots, N$, it can be concluded that the synchronization manifold $\boldsymbol{X}_s$ is stable, which means that the studied network can achieve synchrony. In our case, since $\lambda_i = N$ for $i = 2, \ldots, N$, Network (4) can achieve synchrony as soon as $\Psi(K) < 0$ for $\lambda_2 = N$. Fig. 2a demonstrates the MLE of the Network (11) for $0 \leq K \leq 0.05$. Furthermore, the time-averaged synchronization error is obtained numerically and shown in Fig. 2b. It should be noted that the initial conditions are selected so that all oscillators behave chaotically in $K = 0$.

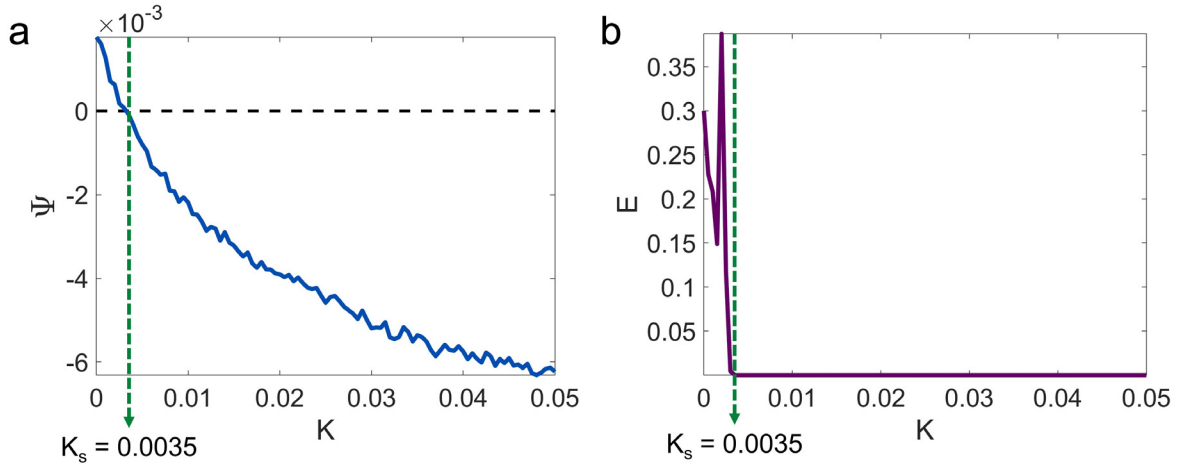

Fig. 2. (a) The MSF and (b) the time-averaged synchronization error of Network (4), for $0 \leq K \leq 0.05$. In this case, the two-level laser oscillators are coupled via linear diffusive couplings in an all-to-all network configuration with N = 100. The oscillators achieve synchrony in $K \geq 0.0035$. The initial conditions are selected so that all oscillators exhibit chaotic behaviors in $K = 0$.

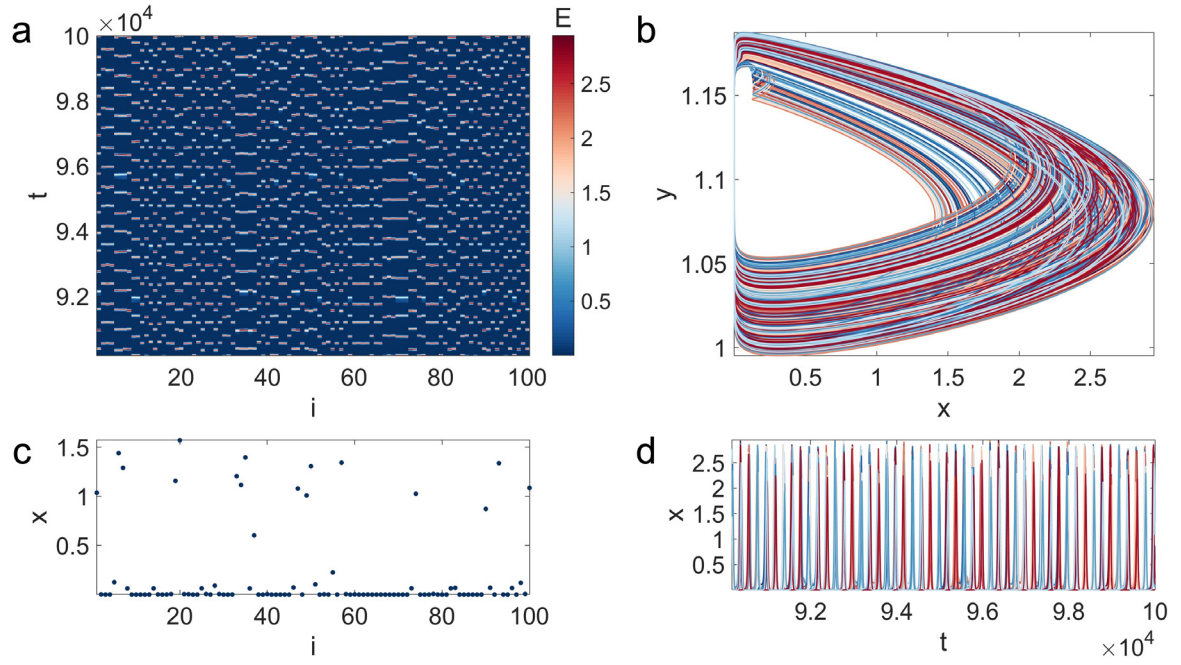

Fig. 3. (a) The spatio-temporal pattern, (b) the phase portraits, (c) the snapshot of the last sample, and (d) the time-series of $N = 100$ laser models coupled via the linear diffusive coupling function in a global coupling network structure (Network (4)) for $K = 4 \times 10^{-7}$. In this coupling parameter K, the oscillators reach the chimera state.

Fig. 2 depicts that in the studied network (Network (4)), the coupled oscillators (through the linear diffusive coupling function) achieve complete synchrony as soon as the coupling parameter K reaches the critical value of $K_s = 0.0035$. Before getting synchronous ($0 \leq K < 0.0035$), Network (4) is investigated to find other synchronization patterns, such as the chimera state, wherein the coherent cluster coexists with the incoherent one, solitary state, wherein all oscillators behave synchronously except for a few oscillators with a state different from the state of synchronous oscillators, and cluster synchronization, wherein some coherent synchronous clusters coexist. Fig. 3 represents that through the linear diffusive coupling function in the global structure, the oscillators can become partially synchronized and reach the chimera state for $K = 4 \times 10^{-7}$. In the same framework, as shown in Fig. 4, another partial synchronization state, namely the solitary state, is observed for $K = 1 \times 10^{-3}$. Furthermore, two-cluster synchronization is found for $K = 2 \times 10^{-3}$, which is illustrated in Fig. 5.

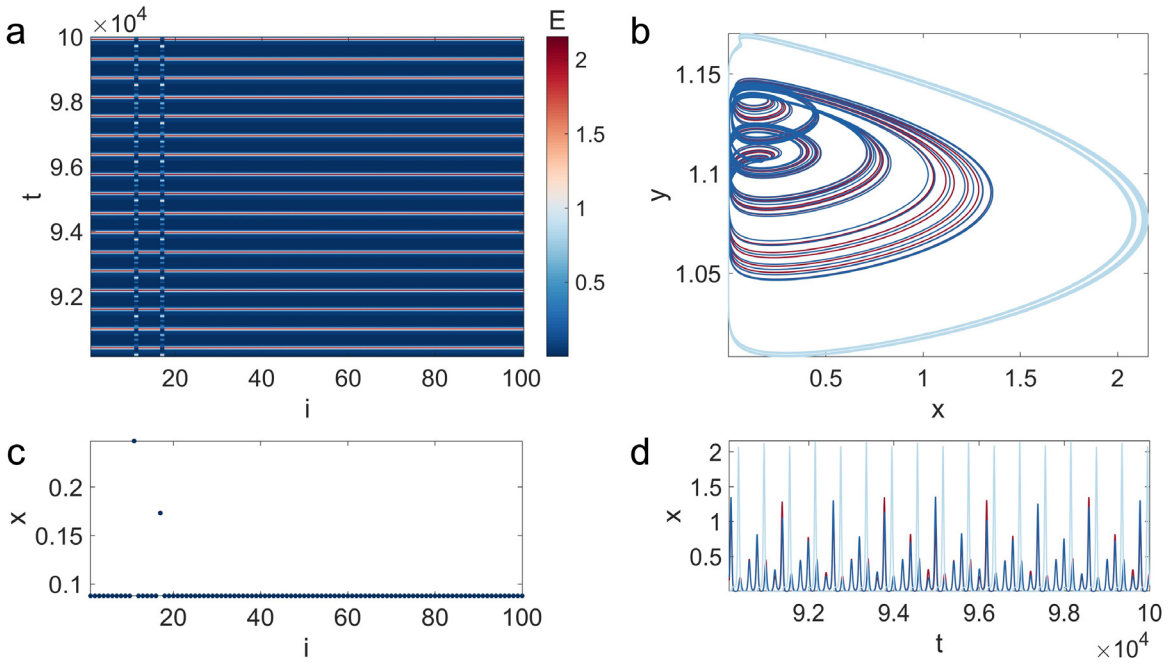

Fig. 4. (a) The spatio-temporal pattern, (b) the phase portraits, (c) the snapshot of the last sample, and (d) the time-series of $N = 100$ laser models coupled via the linear diffusive coupling function in a global coupling network structure (Network (4)) for $K = 1 \times 10^{-3}$. In this coupling parameter K, the oscillators reach the solitary state.

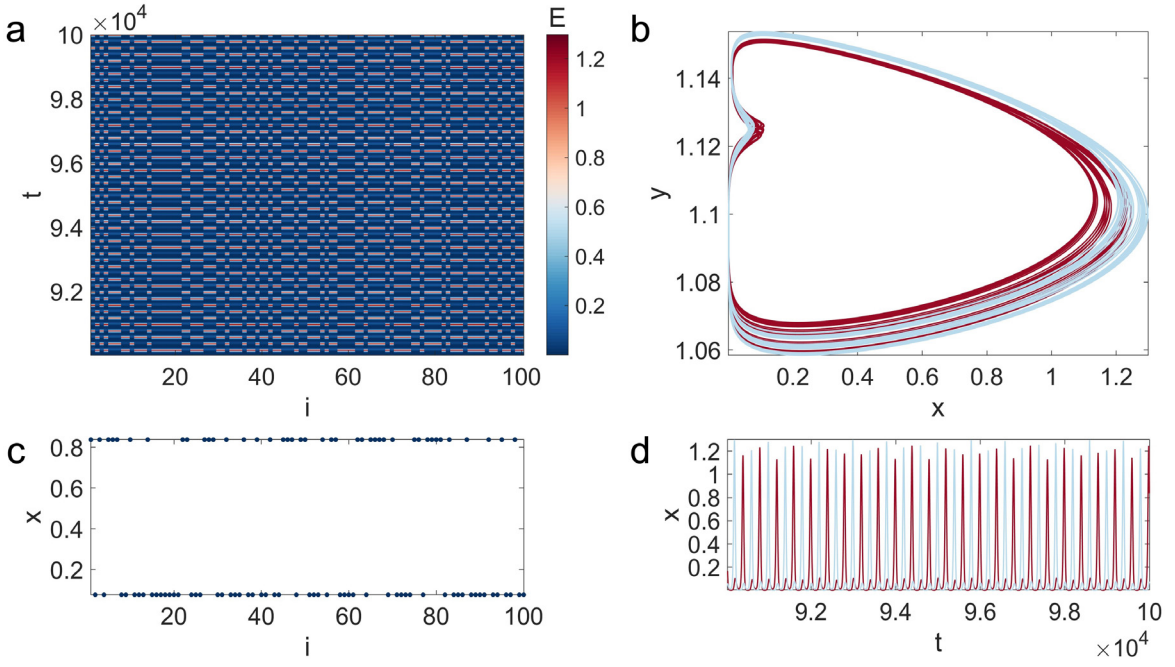

Fig. 5. (a) The spatio-temporal pattern, (b) the phase portraits, (c) the snapshot of the last sample, and (d) the time-series of $N = 100$ laser models coupled via the linear diffusive coupling function in a global coupling network structure (Network (4)) for $K = 2 \times 10^{-3}$. In this coupling parameter K, the oscillators reach the two-cluster synchronization state.

In dynamical system analysis, multistability refers to the concurrent coexistence of various attractors in a similar parameter set [36]. Likewise, in network analysis, multistability denotes the coexistence of multiple manifolds/attractors, either synchronous or asynchronous, to which some network oscillators are attracted. Looking more closely at Fig. 3, it

can be seen that the incoherent cluster contains different periodic attractors (some are period-1, and others are period-2). Thus, the system is multistable in the chimera state. The multistability can also be found in the solitary state shown in Fig. 4. It can be noticed that two oscillators behave chaotically and asynchronously whilst others behave periodically in a synchronous period-2 manifold. The coexistence of two synchronous chaotic manifolds can be observed in the two-cluster synchronization state demonstrated in Fig. 5.

3.2. Nonlinear diffusive coupling function

In the second scenario, the diffusive term is assumed to affect the modulation signal, which is more sensible in laser physics due to the stimulation of cavity losses. Thus, we have $I_m \rightarrow I_m + \epsilon \sum_{j=1}^{N} G_{ij}(x_j - x_i)$. Accordingly, Network (1) can be modified as

$$\dot{\boldsymbol{X}}_i = \begin{cases} \dot{x}_i = -x_i \left(1 + k \left(I_m \right. \right. \\ \left. \left. + \epsilon \sum_{j=1}^{N} G_{ij}(x_j - x_i) \right)^2 - y_i \right) \\ \dot{y}_i = -\gamma y_i - \alpha x y_i + \gamma p_0 \end{cases} . \tag{12}$$

The above-mentioned Network (12) can be simplified as

$$\dot{\boldsymbol{X}}_i = \begin{cases} \dot{x}_i = -x_i(1 + kI_m^2 - y_i) \\ -kx_i \left(\epsilon \sum_{j=1}^{N} G_{ij}(x_j - x_i) \right)^2 \\ -2kI_m x_i \epsilon \sum_{j=1}^{N} G_{ij}(x_j - x_i) \\ \dot{y}_i = -\gamma y_i - \alpha x y_i + \gamma p_0 \end{cases} . \tag{13}$$

Hence, in this case, the diffusive term impacts the network dynamics nonlinearly, and the coupling function $\boldsymbol{H}(\boldsymbol{X}_i, \boldsymbol{X}_j)$ can be defined as two separate functions $\boldsymbol{H}_1(\boldsymbol{X}_i, \boldsymbol{X}_j)$ with the strength of $-k\epsilon^2$ and $\boldsymbol{H}_2(\boldsymbol{X}_i, \boldsymbol{X}_j)$ with the strength of $-2kI_m\epsilon$ as

$$\begin{aligned} &\boldsymbol{H}_1(\boldsymbol{X}_i, \boldsymbol{X}_j) = [x_i(x_j - x_i)^2, 0], \\ &\boldsymbol{H}_2(\boldsymbol{X}_i, \boldsymbol{X}_j) = [x_i(x_j - x_i), 0]. \end{aligned} \tag{14}$$

The synchronizability of Network (13) is examined using the MSF analysis, which is an analytical approach to synchronization. Knowing the fact that $\boldsymbol{X}_1 = \boldsymbol{X}_2 = \cdots = \boldsymbol{X}_{N-1} = \boldsymbol{X}_N = \boldsymbol{X}_s$, in the synchronization state, we have $\boldsymbol{H}_1(\boldsymbol{X}_i, \boldsymbol{X}_j) = \boldsymbol{H}_2(\boldsymbol{X}_i, \boldsymbol{X}_j) \equiv 0$, and similar to the previous case, the synchronization manifold becomes

$$\boldsymbol{F}(\boldsymbol{X}_s) = \begin{cases} f(x_s, y_s) = -x_s(1 + kI_m^2 - y_s) \\ g(x_s, y_s) = -\gamma y_s - \alpha x y_s + \gamma p_0 \end{cases} , \tag{15}$$

which is similar to the dynamics of an isolated decoupled oscillator. To implement the MSF analysis, a negligible perturbation $\delta\boldsymbol{X}_i$, where $\delta\boldsymbol{X}_i = (\delta x_i, \delta y_i)$, is rolled up to the synchronization manifold $\boldsymbol{X}_s$, where $\boldsymbol{X}_s = (x_s, y_s)$. Therefore, $\delta\boldsymbol{X}_i = \boldsymbol{X}_i - \boldsymbol{X}_s$. Consequently, the dynamics of the perturbation equations can be obtained through

$$\begin{aligned} &\delta\dot{\boldsymbol{X}}_i = \boldsymbol{DF}(\boldsymbol{X}_s)\delta\boldsymbol{X}_i - \\ &k\epsilon^2 \sum_{j=1}^{N} G_{ij} \\ &\left[\frac{\partial \boldsymbol{H}_1}{\partial \boldsymbol{X}_i}\bigg|_{(\boldsymbol{X}_s, \boldsymbol{X}_s)} \delta\boldsymbol{X}_i + \frac{\partial \boldsymbol{H}_1}{\partial \boldsymbol{X}_j}\bigg|_{(\boldsymbol{X}_s, \boldsymbol{X}_s)} \delta\boldsymbol{X}_j \right] - \\ &2kI_m\epsilon \sum_{j=1}^{N} G_{ij} \\ &\left[\frac{\partial \boldsymbol{H}_2}{\partial \boldsymbol{X}_i}\bigg|_{(\boldsymbol{X}_s, \boldsymbol{X}_s)} \delta\boldsymbol{X}_i + \frac{\partial \boldsymbol{H}_2}{\partial \boldsymbol{X}_j}\bigg|_{(\boldsymbol{X}_s, \boldsymbol{X}_s)} \delta\boldsymbol{X}_j \right]. \end{aligned} \tag{16}$$

Here, $\boldsymbol{DF}(\boldsymbol{X}_s)$ is the Jacobian matrix of $\boldsymbol{F}(\boldsymbol{X}_i)$ in the synchronization state $\boldsymbol{X}_s$. Considering the definition of $\boldsymbol{H}_1(\boldsymbol{X}_i, \boldsymbol{X}_j)$ and $\boldsymbol{H}_2(\boldsymbol{X}_i, \boldsymbol{X}_j)$ given in Eq. (14), the perturbation equation presented in Eq. (16) turns into

$$\delta\dot{\boldsymbol{X}}_i = \begin{cases} \delta\dot{x}_i = Df(\boldsymbol{X}_s)\delta\boldsymbol{X}_i \\ -2kI_m x_s \epsilon \sum_{j=1}^{N} G_{ij}\left(\delta x_j - \delta x_i\right) \\ \delta\dot{y}_i = Dg(\boldsymbol{X}_s)\delta\boldsymbol{X}_i \end{cases}, \tag{17}$$

where A is a diagonal matrix containing the nodes' degree on its main diagonal, L is the Laplacian matrix obtained from $L = A - G$. As a result, $\delta\dot{x}_i$ formulated in Eq. (17) can be rewritten in terms of the Laplacian matrix L as follows

$$\begin{aligned} &\delta\dot{x}_i = Df(\boldsymbol{X}_s)\delta\boldsymbol{X}_i \\ &-2kI_m x_s \epsilon \sum_{j=1}^{N} G_{ij}\delta x_j + 2kI_m x_s \epsilon \sum_{j=1}^{N} G_{ij}\delta x_i \\ &= Df(\boldsymbol{X}_s)\delta\boldsymbol{X}_i \\ &-2kI_m x_s \epsilon \left(\sum_{j=1}^{N} A_{ij}\delta x_j - \sum_{j=1}^{N} L_{ij}\delta x_j\right) \\ &+2kI_m x_s \epsilon \delta x_i \sum_{j=1}^{N} G_{ij} \\ &= Df(\boldsymbol{X}_s)\delta\boldsymbol{X}_i \\ &-2kI_m x_s \epsilon \left((N-1)\delta x_i - \sum_{j=1}^{N} L_{ij}\delta x_j\right) \\ &+2kI_m x_s \epsilon (N-1)\delta x_i \\ &= Df(\boldsymbol{X}_s)\delta\boldsymbol{X}_i + 2kI_m x_s \epsilon \sum_{j=1}^{N} L_{ij}\delta x_j. \end{aligned} \tag{18}$$

The aforementioned Eq. (18) is inherently in a block diagonally coupled form that can be simplified (block diagonally decoupled) by diagonalizing the eigenvalues of the Laplacian matrix L as

$$\delta\dot{\boldsymbol{X}}_i = \begin{cases} \delta\dot{x}_i = Df(\boldsymbol{X}_s)\delta\boldsymbol{X}_i + 2kI_m x_s \epsilon \lambda_i \delta x_i \\ \delta\dot{y}_i = Dg(\boldsymbol{X}_s)\delta\boldsymbol{X}_i \end{cases}. \tag{19}$$

Here λ_i is the eigenvalues of the Laplacian matrix L. Letting $\delta\boldsymbol{X}_i : (\delta x_i, \delta y_i) \rightarrow \boldsymbol{\zeta}_i : (\zeta_i^x, \zeta_i^y)$ and considering $K_i = \epsilon\lambda_i$, where K is the normalized coupling parameter, the perturbation equation reads

$$\delta\dot{\boldsymbol{\zeta}}_i = \begin{cases} \delta\dot{\zeta}_i^x = f_x\zeta_i^x + f_y\zeta_i^y + 2kI_m x_s K_i \zeta_i^x \\ \delta\dot{\zeta}_i^y = g_x\zeta_i^x + g_y\zeta_i^y \end{cases}. \tag{20}$$

As mentioned above, due to homogeneity and all-to-all configuration, we have $\lambda_1 = 0$, and $\lambda_2 = \lambda_3 = \cdots = \lambda_{N-1} = \lambda_N = N$. Accordingly, the MLE of Network (20) results in the MSF (Ψ). The negative sign of Ψ shows the stability of the synchronization manifold.

Fig. 6a analytically shows that the oscillators coupled through the nonlinear diffusive coupling in an all-to-all network design cannot get synchronous completely. Although the time-averaged synchronization error depicted in Fig. 6b tends to reach zero as the coupling parameter K increases, it never touches the zero line. Our investigation reveals that as the parameter K grows gradually, two synchronous clusters, including a fixed point and a periodic (period-1) manifold, are formed (for $0.5 \leq K \leq 100$). This two-cluster synchronization state can be observed in Fig. 7 for $K = 95$. The more the parameter increments, the slighter the distance between the two manifolds.

Based on the definition of the network multistability mentioned above, the coexistence of a fixed point and a synchronous periodic manifold can be observed in Fig. 7, representing the two-cluster synchronization. More investigations on Network (13) reveal that in some negligible values of the parameter K, the chimera state can be observed, which is shown in Fig. 8 ($K = 1 \times 0^{-3}$). Fig. 8 illustrates different coexisting chaotic attractors, including synchronous and asynchronous clusters.

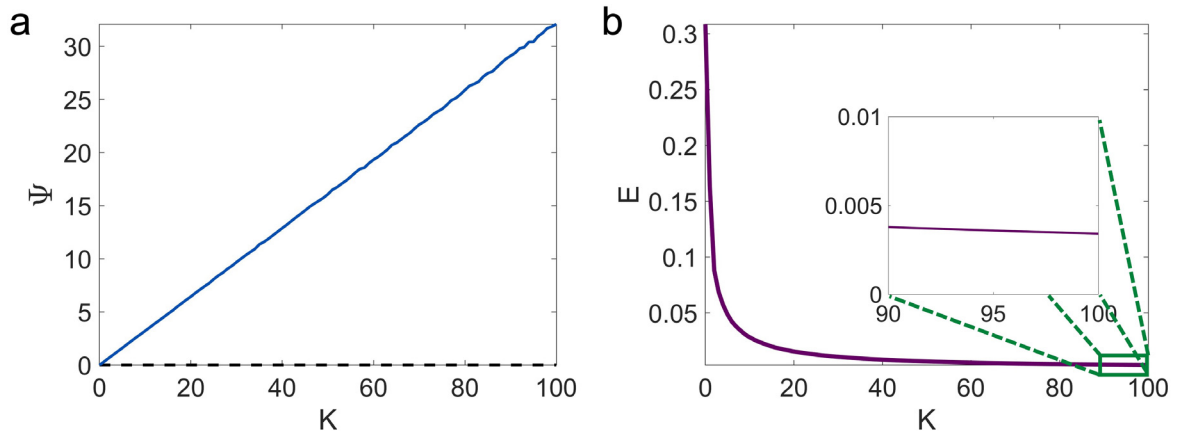

Fig. 6. (a) The MSF and (b) the time-averaged synchronization error of Network (13), for $0 \leq K \leq 100$. In this case, the two-level laser oscillators are coupled via nonlinear diffusive couplings in an all-to-all network configuration with $N = 100$. The oscillators do not achieve synchrony in the studied interval of parameter K. The initial conditions are selected so that all oscillators exhibit chaotic behaviors in $K = 0$.

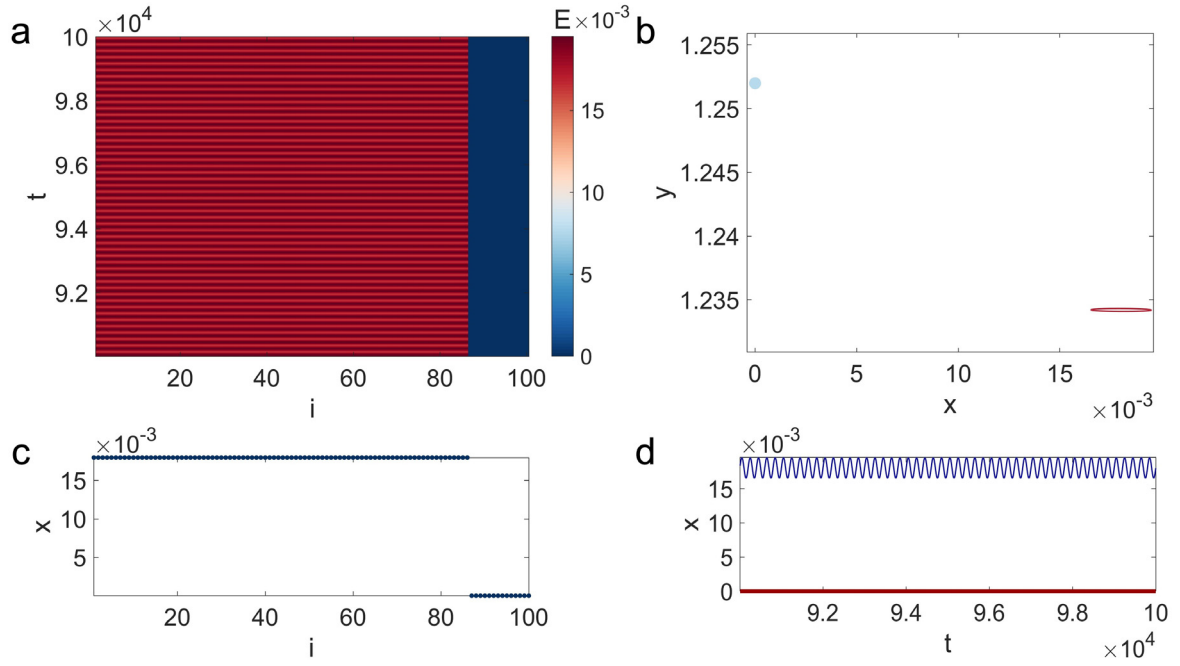

Fig. 7. (a) The spatio-temporal pattern, (b) the phase portraits, (c) the snapshot of the last sample, and (d) the time-series of $N = 100$ laser models coupled via the nonlinear diffusive coupling function in a global coupling network structure (Network (13)) for $K = 95$. In this coupling parameter K, the oscillators reach the two-cluster synchronization state.

4. Conclusions

Due to the importance of laser synchronization in information communication, this paper investigated the synchronization of a network of coupled laser models with shift-invariant couplings. To accomplish this purpose, 100 identical laser models were considered to interact in an all-to-all network configuration with diffusive coupling functions in two scenarios: linear and nonlinear definitions. The laser model employed as the dynamics of the network units was recently introduced in [33]. In each case, the analytical (through the MSF analysis) and numerical (using the time-averaged synchronization error) approaches were performed. The results showed that, in the linear case, the interacting laser models reach a common temporal pattern in a negligible value of the coupling parameter ($K = 0.0035$). However, the studied network exhibited rich dynamical properties as we found chimera, solitary state, and two-cluster synchronization patterns before achieving complete synchrony. The recognized patterns were all multistable since there existed more than

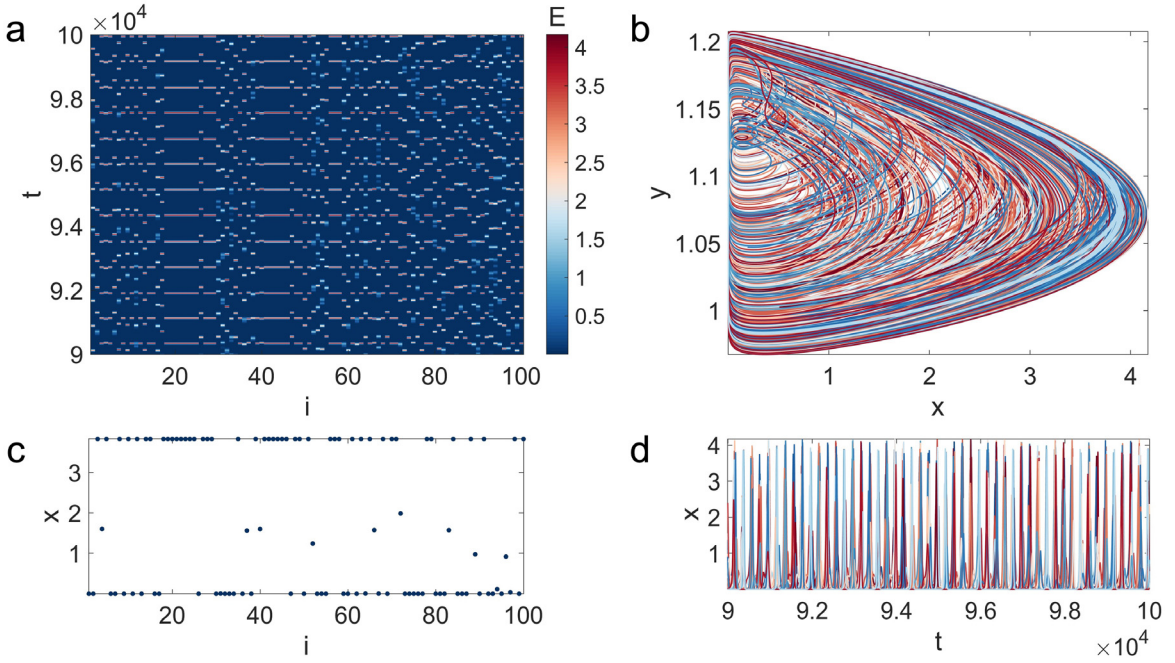

Fig. 8. (a) The spatio-temporal pattern, (b) the phase portraits, (c) the snapshot of the last sample, and (d) the time-series of $N = 100$ laser models coupled via the nonlinear diffusive coupling function in a global coupling network structure (Network (13)) for $K = 1 \times 10^{-3}$. In this coupling parameter K, the oscillators reach the chimera state.

one solution to the model. Unlike the linear case, in the nonlinear diffusive scheme, based on the MSF and synchronization error results, complete synchronization was unachievable. Yet, in a considerable range of the coupling parameter, the coupled models become synchronous in two clusters, namely a fixed point and a periodic orbit. Also, in small values of the coupling parameter K, multistable chimera patterns were observed.

In the presented paper, similar to Kouomou and Woafo [31], the laser models were bidirectionally and diffusively coupled but in a one-dimensional global configuration. However, two types of diffusive coupling functions, namely, linear and nonlinear diffusive functions, were studied. As a result, in the nonlinear case, we found the formation of two clusters in the higher coupling coefficient values. The formation of two synchronous clusters was also found in the linear case in the lower value of the coupling parameter. This is also in line with the results reported by Röhm et al. [32], although the effect of the delay was not involved in the present study. On the other hand, we found multistable chimera states in both studied cases. Unlike [27,29], we found neither lag synchronization nor phase synchronization patterns. However, as a future study, the formation of various synchronization patterns can be examined by considering the network of delay-coupled laser models or considering the master–slave configuration (similar to [25,26]).

CRediT authorship contribution statement

Mahtab Mehrabbeik: Software, Visualization, Writing – original draft. **Sajad Jafari:** Methodology, Validation, Writing – original draft. **Riccardo Meucci:** Conceptualization, Supervision, Writing – review & editing. **Matjaž Perc:** Supervision, Validation, Writing – review & editing.

Declaration of competing interest

The authors declare that they have no known competing financial interests or personal relationships that could have appeared to influence the work reported in this paper.

Data availability

No data was used for the research described in the article

References

[1] Boccaletti S, Latora V, Moreno Y, Chavez M, Hwang D-U. Complex networks: Structure and dynamics. Phys Rep 2006;424:175–308.
[2] Caruntu DI, Taylor KN. Nonlinear dynamics of electrostatically actuated coupled mems parallel cantilever resonators. In: International design engineering technical conferences and computers and information in engineering conference, Vol. 45004. American Society of Mechanical Engineers; p. 897–902.
[3] Parastesh F, Mehrabbeik M, Rajagopal K, Jafari S, Perc M. Synchronization in Hindmarsh–Rose neurons subject to higher-order interactions. Chaos 2022;32:013125.
[4] Boccaletti S, Kurths J, Osipov G, Valladares D, Zhou C. The synchronization of chaotic systems. Phys Rep 2002;366:1–101.
[5] Kocamaz UE, Çiçek S, Uyaroğlu Y. Secure communication with chaos and electronic circuit design using passivity-based synchronization. J Circuits Syst Comput 2018;27:1850057.
[6] Khitun A, Bao M, Lee J-Y, Wang KL, Lee DW, Wang SX, Roshchin IV. Inductively coupled circuits with spin wave bus for information processing. J Nanoelectron Optoelectron 2008;3:24–34.
[7] Chavez M, Hwang DU, Boccaletti S. Synchronization processes in complex networks. Eur Phys J Spec Top 2007;146:129–44.
[8] Ghosh D, Frasca M, Rizzo A, Majhi S, Rakshit S, Alfaro-Bittner K, Boccaletti S. The synchronized dynamics of time-varying networks. Phys Rep 2022;949:1–63.
[9] Rybalova E, Strelkova G, Schöll E, Anishchenko V. Relay and complete synchronization in heterogeneous multiplex networks of chaotic maps. Chaos 2020;30:061104.
[10] Pecora LM, Carroll TL. Master stability functions for synchronized coupled systems. Phys Rev Lett 1998;80:2109–12.
[11] Buscarino A, Fortuna L, Frasca M, Sciuto G. Chua's circuits synchronization with diffusive coupling: New results. Int J Bifurcation Chaos 2009;19:3103–7.
[12] Majhi S, Perc M, Ghosh D. Dynamics on higher-order networks: A review. J R Soc Interface 2022;19:20220043.
[13] Hussain I, Jafari S, Ghosh D, Perc M. Synchronization and chimeras in a network of photosensitive Fitzhugh–Nagumo neurons. Nonlinear Dynam 2021;104:2711–21.
[14] Parastesh F, Jafari S, Azarnoush H, Shahriari Z, Wang Z, Boccaletti S, Perc M. Chimeras. Phys Rep 2021;898:1–114.
[15] Gambuzza LV, Buscarino A, Chessari S, Fortuna L, Meucci R, Frasca M. Experimental investigation of chimera states with quiescent and synchronous domains in coupled electronic oscillators. Phys Rev E 2014;90:032905.
[16] Rybalova E, Anishchenko V, Strelkova G, Zakharova A. Solitary states and solitary state chimera in neural networks. Chaos 2019;29:071106.
[17] Zhang L, Pan W, Yan L, Luo B, Zou X, Li S. Strong cluster synchronization in complex semiconductor laser networks with time delay signature suppression. Opt Express 2022;30:30727–38.
[18] Weiner JM, Cox KC, Bohnet JG, Thompson JK. Phase synchronization inside a superradiant laser. Phys Rev A 2017;95:033808.
[19] Shahverdiev EM, Sivaprakasam S, Shore KA. Lag synchronization in time-delayed systems. Phys Lett A 2002;292:320–4.
[20] Agrawal GP. Effect of gain nonlinearities on period doubling and chaos in directly modulated semiconductor lasers. Appl Phys Lett 1986;49:1013–5.
[21] Ciofini M, Labate A, Meucci R, Galanti M. Stabilization of unstable fixed points in the dynamics of a laser with feedback. Phys Rev E 1999;60:398–402.
[22] Meucci R, Euzzor S, Tito Arecchi F, Ginoux J-M. Minimal universal model for chaos in laser with feedback. Int J Bifurcation Chaos 2021;31:2130013.
[23] Pecora LM, Carroll TL. Synchronization in chaotic systems. Phys Rev Lett 1990;64:821.
[24] Uchida A, Rogister F, García-Ojalvo J, Roy R. Synchronization and communication with chaotic laser systems.
[25] Sugawara T, Tachikawa M, Tsukamoto T, Shimizu T. Observation of synchronization in laser chaos. Phys Rev Lett 1994;72:3502–5.
[26] Mariño IP, Allaria E, Sanjuán MAF, Meucci R, Arecchi FT. Coupling scheme for complete synchronization of periodically forced chaotic CO_2 lasers. Phys Rev E 2004;70:036208.
[27] DeShazer DJ, Breban R, Ott E, Roy R. Detecting phase synchronization in a chaotic laser array. Phys Rev Lett 2001;87:044101.
[28] Hillbrand J, Auth D, Piccardo M, Opačak N, Gornik E, Strasser G, Capasso F, Breuer S, Schwarz B. In-phase and anti-phase synchronization in a laser frequency comb. Phys Rev Lett 2020;124:023901.
[29] Mihana T, Fujii K, Kanno K, Naruse M, Uchida A. Laser network decision making by lag synchronization of chaos in a ring configuration. Opt Express 2020;28:40112–30.
[30] Zhang L, Pan W, Yan L, Luo B, Zou X, Xu M. Cluster synchronization of coupled semiconductor lasers network with complex topology. IEEE J Sel Top Quant Electron 2019;25:1–7.
[31] Chembo Kouomou Y, Woafo P. Cluster synchronization in coupled chaotic semiconductor lasers and application to switching in chaos-secured communication networks. Opt Commun 2003;223:283–93.
[32] Röhm A, Böhm F, Lüdge K. Small chimera states without multistability in a globally delay-coupled network of four lasers. Phys Rev E 2016;94:042204.
[33] Meucci R, Marc Ginoux J, Mehrabbeik M, Jafari S, Clinton Sprott J. Generalized multistability and its control in a laser. Chaos 2022;32:083111.
[34] Heagy JF, Carroll TL, Pecora LM. Synchronous chaos in coupled oscillator systems. Phys Rev E 1994;50:1874–85.
[35] Huang L, Chen Q, Lai Y-C, Pecora LM. Generic behavior of master-stability functions in coupled nonlinear dynamical systems. Phys Rev E 2009;80:036204.
[36] Li C, Wang X, Chen G. Diagnosing multistability by offset boosting. Nonlinear Dynam 2017;90:1335–41.